Student Organization for Aerospace Research Atlantis II Sounding Rocket

Team 43 Project Technical Report for the 2018 IREC

J. Martens[1], X. Cui[2], H. Stoldt[3], L. Alacoque[4], T. Messinger[5], A. Hamilton[6], Wm. K. van der Meulen[7], A. Deshpande[8]
University of Calgary, Calgary, AB, T2L 1B3, Canada

The following report details the hybrid powered sounding rocket design put forth by the Student Organization for Aerospace Research (SOAR) at the University of Calgary. The sounding rocket officially known as Atlantis II, is SOAR's entry into the 2018 Intercollegiate Rocket Engineering Competition at Spaceport America, New Mexico. SOAR's vision is for Atlantis II to achieve a target altitude of 30,000-feet above ground level. To accomplish this task, Atlantis II is powered by a student researched and designed hybrid rocket motor using paraffin wax as fuel, and nitrous oxide as an oxidizer. The rocket measures 17 feet in length, and 7 inches in diameter, and will be carrying an 8.8 lb scientific payload. This payload aims to measure the efficacy of different materials used to shield humans, and other biological systems, from the increased levels of radiation in space. A new composite material was developed by the University of Calgary to be usable for space wear while providing the required radiation shielding - specifically, the range of radiation that composes "cosmic radiation". Our payload also records the temperature distribution along the length of the rocket nose cone, and collects flight spin and speed information. This data, in combination with acceleration, GPS and barometer data from our main avionics system, will be highly valuable in improving our overall rocket and engine design.

[1] Undergraduate, Mechanical Engineering, 2500 University Dr NW, Calgary, AB T2N 1N4
[2] Undergraduate, Mechanical Engineering, 2500 University Dr NW, Calgary, AB T2N 1N4
[3] Undergraduate, Mechanical Engineering, 2500 University Dr NW, Calgary, AB T2N 1N4
[4] Undergraduate, Mechanical Engineering, 2500 University Dr NW, Calgary, AB T2N 1N4
[5] Undergraduate, Mechanical Engineering, 2500 University Dr NW, Calgary, AB T2N 1N4
[6] Undergraduate, Mechanical Engineering, 2500 University Dr NW, Calgary, AB T2N 1N4
[7] Undergraduate, Electrical Engineering and Computer Science, 2500 University Dr NW, Calgary, AB T2N 1N4
[8] Undergraduate, Mechanical Engineering, 2500 University Dr NW, Calgary, AB T2N 1N4

Nomenclature

Fy	=	Y component of the resultant pressure force acting on the vehicle
m_{dry}	=	mass of rocket when descending
a	=	acceleration
v_o	=	opening velocity
v_{term}	=	terminal velocity
$SA/inch$	=	Shear area per inch
π	=	pi
D_{max}	=	maximum minor diameter of the internal thread
D_{min}	=	minimum pitch diameter of the external threads
N	=	threads per inch
$\dot{m}_{spi}$	=	mass flow rate single phase flow
$\dot{m}_{hem}$	=	mass flow rate at homogeneous equilibrium
$A_{injection}$	=	Area of the injection plate orifices
ρ	=	density
ΔP	=	Pressure differential
S_n	=	Entropy at location n
$\dot{m}_{Dyer}$	=	Dyer mass flow equation for non-homogeneous non-equilibrium
κ	=	kappa, non-equilibrium parameter
Δh	=	change in enthalpy
t_{cr}	=	thickness of combustion casing
P	=	Pressure
R	=	Radius for combustion chamber equations
S	=	cylindrical stress
e	=	efficiency
C_nH_{2n+1}	=	chemical formula for paraffin wax with n=20-30
A_t	=	nozzle throat area
A_1	=	nozzle inlet area
A_e	=	nozzle exit area
A_p	=	parachute nominal area
M_1	=	Mach number at nozzle inlet
M_t	=	Mach number at nozzle throat
M_e	=	Mach number at nozzle exit
k	=	specific heat ratio
σ	=	dimensionless factor accounting for variation of row and mu values across boundary layer
h_g	=	heat transfer coefficient
T_w	=	wall temperature
T_o	=	stagnation temperature
γ	=	ratio of specific heats in heat transfer equations
ϖ	=	temperature exponent of viscosity equation
Pr	=	Prandtl number
r_c	=	throat radius of curvature
μ	=	viscosity
g	=	gravitational acceleration
D^*	=	throat diameter for heat transfer equations
A^*	=	throat area for heat transfer equations
C^*	=	characteristic velocity for heat transfer equations
C_p	=	specific heat at constant pressure
C_d	=	Coefficient of drag

I. Introduction

The Atlantis II sounding rocket is the Student Organization for Aerospace Research's (SOAR's) entry in the 2018 Intercollegiate Rocket Engineering Competition (IREC) at Spaceport America, New Mexico. The Atlantis II will be the third sounding rocket that SOAR has entered into the IREC event over the years, featuring SOAR's second SRAD motor, making it the second SOAR rocket attempting a target altitude of 30,000-feet. In 2016, SOAR entered it's first IREC event with a basic Commercial off the Shelf (COTS) rocket that reached an altitude of 9,200-feet, and placed middle of the group at 22 out of 40 teams. For the 2017 competition, SOAR entered a new rocket, a Student Researched and Developed (SRAD) hybrid rocket. This rocket placed 3rd in its category.

SOAR is run and operated by students from multiple disciplines and faculties including mechanical engineering, electrical engineering, physics, and computer science. The team has two academic advisors, Dr. Craig Johansen from Mechanical Engineering, and Dr. Chris Cully from the Faculty of Science. SOAR is an extracurricular club where students do not receive any additional credits for their work but instead have the opportunity to reinforce engineering principles learned in class and apply them to real-world aerospace applications with time and resource constraints. SOAR helps students gain experience in manufacturing, design, teamwork, and project management - an opportunity that is not readily offered in the classroom. SOAR has positioned itself to thrive in the future with strong support from academic advisors, an aerospace sponsor, core team members, and new recruits.

The objective of the club is to provide members with the ability to learn about physics and engineering with a hands-on approach. The projects provide education in space sciences through the creation and completion of various projects from start to finish. The club also creates awareness on campus about space research at the University of Calgary, as well as related projects from the Canadian Space Agency with the intent to further student knowledge and motivate/interest future researchers.

The Atlantis II rocket name was chosen to signify that this is the team's second iteration of this size and class of rocket. The project has numerous stakeholders that offered valuable resources and knowledge needed to complete the Atlantis II hybrid sounding rocket. The project received generous contributions from the University of Calgary Schulich School of Engineering and from the Faculty of Science, who provided funding, workspace, and resources necessary to attend the competition in New Mexico. SOAR also received a significant amount of help and materials from the fantastic team at Luxfer Gas Cylinders in Calgary. Lastly, the University of Calgary Rothney Astrophysical Observatory generously donated the space in their static test facility for SOAR's use.

II. System Architecture Overview

The Atlantis II is a 17-foot length, 7-inch diameter sounding rocket with a target altitude of 30,000-feet., primarily made of student researched and designed components. The exterior of the rocket is made out of two carbon fiber filament wound body tubes and a composite overwrapped pressure vessel (carbon fiber wrapped on an aluminum 6061-T6 liner) as the oxidizer tank. The top section of the rocket comprises a fiberglass composite nose cone with an aluminum tip, drogue parachute and a scientific payload. The top carbon fiber tube contains the main parachute, avionics and recovery systems. A 7-foot pressure vessel makes up the middle section of the rocket where the nitrous oxide oxidizer is contained. This section attaches to the combustion chamber assembly via a radial - axial joint. The aluminum combustion chamber assembly is encased by a carbon fiber body tube, which houses the injector feed system, combustion chamber, fuel grain, motor control system, and nozzle. Three symmetric and replaceable clipped delta fins made out of basswood wrapped with multiple layers of carbon fiber are bolted through the rocket body tube.

Figure 1: Cross-sectional view of the Atlantis II sounding rocket.

A. Aero-structures Subsystems

1.1 Nose Cone

The shape of the nose cone was determined using OpenRocket, a rocket simulation software that was used to model the Atlantis II. Identical simulations were executed with varying nose geometry and the results were analyzed in the areas of drag, velocity and acceleration. Shown below is a table outlining the primary results and ultimate decision of designing a nose cone with ½ Power geometry. Furthermore the fineness ratio had to be analysed to conclude the optimal length to diameter ratio. This analysis was also completed with OpenRocket software in the same manner. The final result was a nose cone modelled with ½ Power series geometry and 6:1 fineness ratio resulting in minimum drag and maximum altitude and velocity (details in Appendix VI).

Table 1: Nose Cone Geometry and Respective Assessment at Varying Mach Speeds

Type of Nose Cone	Optimum Range (Mach) [45]	Drag at Mach 1.2	Surface Area
¾ Power	(0.8-0.9), (1.6-2.2) and 2+	3	1
½ Power	(0.8 -1.8)	1	2
LD Haack Series	(0.8 – 1.35), (1.75- 2.2)	2	3

On a number scale where the larger the number the lower the ranking, i.e. the worse it is in a category in comparison

In conjunction with the connecting body tubes of the Atlantis II the base of the nose cone has a diameter of 7" and corresponding to the 6:1 fineness ratio the final length is 42". This ensured that the internal volume of the nose cone is large enough to house the payload system and consequently reduced the length of body tubes and the rocket's overall weight and surface area.

To determine the potential pressures, heat transfer and overall fluid mechanics of the Atlantis II nose cone the geometry described previously was modelled and simulated in Solidworks and ANSYS software. Upon completing the simulations it was found the largest potential forces were 130 kPa (gauge) at fluid velocities of 450 m/s parallel to length of nose cone and 17 m/s perpendicular. From this data ANSYS composite simulation was conducted to determine that 4 ply of 6 oz E-glass fiberglass and Aeropoxy PR2032 laminating resin was needed to withstand flight loads. Fiberglass was decided upon to ensure the nose cone is radio frequency transparent, lightweight and with high strength capabilities. Maximum temperature was located at the stagnation point at the tip of the rocket and calculated to be 130 _C. An aluminum tip was manufactured to withstand the stagnation temperatures during flight and it was verified that temperatures during flight would be low enough to ensure that the PR2032 epoxy would not reach glass transition state or deform along the length of the nose cone. Details are available in Appendix VI.

1.1.1 Drogue Connection:

The line connecting the nose cone to the drogue chute is threaded through the upper bulkhead at the base of the nose cone. It enters on one side, passes underneath the payload and then exits on the other. Both the entry and exit holes have a rounded profile to avoid having the parachute cord on a sharp 90 degree angle.

1.1.2 Body Tube Connection:

The nose cone connects the upper body tube via a number of small nylon bolts. They bolt into a 3.5" long section of ⅛" wall Aluminum pipe protruding from the upper body tube. One inch of the tube is epoxied permanently into the upper body tube and two and a half inches protrude into the bottom of the nose cone. The nylon bolts are designed to fail in shear when the recovery system is triggered. The number of nylon bolts used modulates the amount of pressure built up in the upper body tube and nose cone before the nose cone is released and will be set through experimental testing.

1.2 Rocket Body Tubes

The SOAR team endeavored to make its own body tubes once again this year. They had to be strong but also light, which made composites very appealing. SOAR had our body tubes filament wound with carbon fiber because

of the superior strength of filament wound tubes. The angle of the windings and the number of layers (4) were based off of the results obtained from ANSYS FEA software and a simulation prepared to test various loading conditions. Due to restrictions imposed by our mandrel and the sponsor's winding setup, the lowest angle we could achieve was 33° (all angle from the longitudinal). Because most of the loads experienced by the body tubes are expected to be axial or bending loads, this became the winding angle for our first layer. The 4th layer (farthest from the center of the cylinder) was set to be 85° to ensure good compression of the interior layers and to give some amount of compressive strength. Since our body tubes will primarily be under axial loading, we considered the following possibilities for the orientation of our winding angles, and tested them using FEA simulations.

Our loading cases are as follows (further info available in Appendix VI):
Flight Loads: Axial Force: -3515N(Compressive) Bending Moment: 231.2 Nm Shear Force: 209.7N
Parachute Deployment Loads: Axial Force: 2920N Bending Moment: 806 Nm Shear Force: 290.4N

The winding orientation which resulted in the highest Factor of Safety - [33,33,33,85]. The results of the different orientation of the winding angles are shown below. Failure of the body tubes was checked against the Maximum Principal Failure Criterion.

Table 2: Factor of Safety for Different Fiber Winding Angles

	Parachute Deployment				Flight Loads			
	Layer 1	Layer 2	Layer 3	Layer 4	Layer 1	Layer 2	Layer 3	Layer 4
33,85,-33,85	15.7	5.3	8.3	3.9	36.2	13.2	19.2	9.0
33,33,33,85	15.5	11.3	7.2	3.1	33.9	26.5	15.6	7.6

The reason why the first winding angle orientation was not chosen despite having a higher minimum Factor of Safety is because of the low Factor of Safety in layer 2 of 5.3 during parachute deployment. Since there will primarily be axial loading, having a layer at 85 would have not provided any support except through it's epoxy strength. With the second orientation there is no layer which is experiencing sudden drop on Factor of Safety. It is also important to note that in these simulations all loads were applied evenly around the entire circumference of the body tube, which would not necessarily be the case in the real rocket, especially for axial loads applied by the motor mount system (see 2.4).

1.3 Radax (radial-axial) Joints

As stated, radax joints are used to couple the rocket sections. Each joint consists of two aluminum (6061-T6) cylinder modules, which are coupled together using 16 #8 steel bolts angled at 30º from the longitudinal axis of the rocket. This design allows any loads which the rocket experiences to be distributed chiefly axially along the bolts; as such, our coupling system effectively withstands high tensile/bending loads during groundwork, parachute deployment, and flight descent [41].

The rocket has two radax joints, one each above and below the main pressure vessel. The length of the radax joints is actually not primarily useful for strength (See Appendix VI) but for the ease of alignment with the rocket body tube that it creates. Because the bottom radax joint is adjacent to the motor mount, which provides a realignment location, the bottom radax joint was designed to be shorter than the top one, which has no such alignment mechanism nearby.

1.4.1 Upper Bulkhead:

The purpose of the upper bulkhead is to hold the payload in the nose cone during flight, but also allow easy removal when on the ground. To accomplish this, we separated it into two parts. One has an L-shaped cross section and is permanently epoxied to the interior of the nose cone and the other is a flat circular plate that connects to the bottom of the threaded rods that make up the main structure of the payload. Nut plates are riveted onto the top of the L-shaped piece, allowing the payload and it's mounting plate to bolt in from the bottom. The peak loading this part

was designed for is the peak drogue loading, calculated at 4500 N, since there is a chance this load could be fully applied to the nose cone if slack remains in the section of line between the nose cone and the main rocket while the section of line between the drogue and the nose cone is already pulled taut.

1.4.2 Lower Bulkhead:

The purpose of the lower bulkhead is to provide a secure attachment location for our parachutes. The structure is designed to hold on to a large centered forged steel eye bolt, positioned at the center of the rocket. It is permanently epoxied into the upper body tube and milled out of piece of solid 6061-T6 aluminum. The epoxy bond gap around the bulkhead and all other components epoxied into the body tubes was left at a slightly large 0.02" since it was known in advance that our body tube mandrel / form is not perfectly round.

1.5 Motor Attachment

The purpose of the motor attachment is to transfer largely axial load from the combustion chamber to the rest of the rocket airframe. Since the section of body tube right above the combustion chamber is made out of fiberglass and we do not have a nice way of filament winding strong fiberglass body tubes, we decided to avoid having the fiberglass take the motor load by connecting the motor mount directly to the carbon fiber tube just above the fiberglass section. The motor's force is carried across the fiberglass body tube by four equally spaced lengths of aluminum square tube, positioned to butt right up against the inner wall of our rocket's body and thereby providing the maximum amount of bending strength.

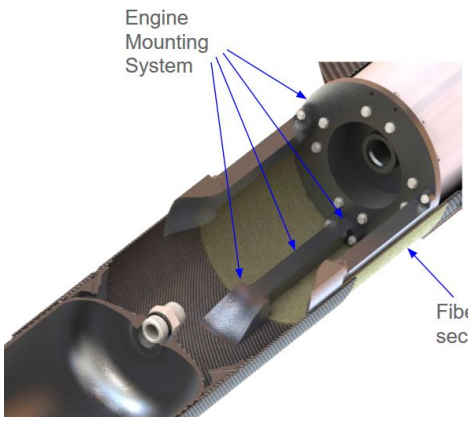

Since our combustion chamber is smaller than the ID of the rocket, an adapter plate was bolted on to the top of the chamber to provide a mounting surface right at the inside wall of the body tube. The square tubes are then bolted both into the adapter plate at the top of the engine and into aluminum blocks permanently epoxied into the rocket just above the transition back to our filament wound carbon fiber body tubes. To make the whole assembly accessible, the bottom body tube, fins and tail fairing can be removed by undoing eight bolts and sliding it off.

Figure 2: Engine Mounting System

1.6 Tail Fairing

The tail fairing will be present simply to ease the transition from the ~7.25" OD rocket body to the smaller diameter combustion chamber exhaust nozzle to allow for less turbulence generated at that point. It will be made from 3-4 layers of 8 HS carbon fiber. It is not expected to take any major loading and so its structure was not verified using composite FEA software, but rather is determined by past composite structure experience. The tail fairing is easily replaceable and attached to the rest of the rocket by three small bond plates and #8 bolts in shear loading.

1.7 Fins

The purpose of the fin design is to create a fin that will provide stability for the rocket through all stages of flight, while at the the same time adding the minimum possible amount of drag. To achieve this, a method for accurately and quickly modelling the rocket stability through different fin iterations was required. OpenRocket software was chosen for this purpose as the primary method for determining stability, and one of two methods for estimating the drag contribution from the fins. Aerolab was used as a secondary source for drag numbers, to compare with OpenRocket, as OpenRocket is not optimized for supersonic calculations [42]. An article in the Apogee newsletter (Why Should You Airfoil Your Rocket's Fins?) mentions that a fin is at its optimum when it is designed with three things – an efficient plan-form, proper symmetrical airfoil, and a precise radial taper. Two main forms of fin planform were examined and contrasted to determine which provided superior aerodynamic properties with equivalent stability. The two planforms were clipped delta and symmetrical trapezoid. Both designs utilized a diamond shaped airfoil, and a radial taper, as mentioned in the Apogee article. OpenRocket simulations showed that with an equal planform area, both geometries provided roughly the same stability throughout ascent, but the clipped

delta design provided a lower drag coefficient in our velocity range. Figures plotting the drag coefficients of each geometry against time are available in Appendix VI.

The pressure drag during the supersonic portion of flight is higher for the Trapezoidal fin. This was verified by running the same geometries through Aerolab. Since drag is related to velocity squared, a model of drag force versus time showed a lower total drag on the clipped delta geometry, which equated to an increased apogee. Due to this, the clipped delta geometry was chosen.

The exact geometry of the fins were then determined in order to satisfy the stability requirements: namely that the rocket be stable at all times throughout the ascent, and always maintain a stability margin between 2.0 and 6.0 (for nominal stability). At the time of the first launch lug departing the launch rail, the rocket is designed to be travelling at a speed of 118ft/s, which is above the minimum speed for launch rail departure stability.

In order to prevent excess drag and stability, a fin mounting system was designed such that multiple different sizes of fins may be attached to the rocket, in order to adapt both to varying wind conditions at launch. An added benefit of this system is that it allows us to adapt quickly and efficiently to changes in the actual rocket weight / CG / CP locations compared to our initial design.

A downside of this mounting system is that due to the requirements for this mounting system, the base of the fin had to be kept identical for each iteration, which constrained some aspects of the geometry, such as sweep angle, at the price of modularity.

The failure case of fin flutter was also examined for our geometry. Critical velocity for fin flutter was calculated using an equation from Apogee Newsletter [43] which is a variation of the equation proposed by Dennis Martin in his NASA paper on flutter calculations [44]. Using this equation, the critical velocity for the fin geometry was calculated to be 787m/s, which is much higher than our maximum velocity of 530m/s.

The structure of the fins consists of a core of laser-cut basswood ribs stacked together to form the desired 3D geometry. To add the required strength, a lay-up of carbon fiber is done. As a means of attaching the fins onto the body tube so that they are easily replaceable, mounting plates are epoxied to the outside of the body tubes. Bolts are then threaded through the mounting plates and into aluminum inserts embedded inside the base of the fins. This system of mounts and fins was designed such that the failure mode will be the bolts in tension, so that any failure can be quickly and easily repaired by simply installing a new set of fins. That failure mode was confirmed to be the one that occurs by a destructive test of a prototype fin.

The three fins will be positioned evenly around the body of the tube by using a CNC routed plywood alignment plate. Then they will be aligned with the body tube's longitudinal axis with a straight slotted piece of sheet metal bent to an angle. With this jig holding the fins and their mounts in position, the mounting plates will be permanently attached allowing replacement of fins with no additional alignment required.

Figure 3: Fin Prototype just prior to failure

B. Recovery Subsystems

2.0 Design

A dual deployment system was chosen for the recovery subsystem of this rocket. This involves the use of a drogue and main parachute and systems to release each parachute. The drogue parachute deployment utilizes two Raptor CO2 systems. This allows for a dual deployment by ejecting the nose cone from the body tube, which simplifies the rocket design by using only one parachute compartment. The main parachute release utilizes a student designed system based off the commercially available Tender Descender [39]. The entire recovery system is shown below in both the drogue parachute deployment stage and the main parachute deployment stage. In addition to the student designed flight computer, a redundant commercially available flight computer powered by a separate battery sends the signals for drogue and main parachute deployment. The commercially available flight computer was chosen to be an Eggtimer Quantum to meet regulation and altitude requirements. When the rocker reaches apogee, the student designed flight computer will send a signal to the two Raptor CO2 systems, pressurizing the parachute compartment to break shear pins that connect the nose to the rocket body. With the nose cone separated, the drogue parachute can deploy. If the first signal fails to trigger the CO2 systems, the Eggtimer will send a delayed signal as backup. Once the rocket descends to an altitude of 1500 ft, a signal and a delayed signal from the Eggtimer are sent

to release the main parachute.

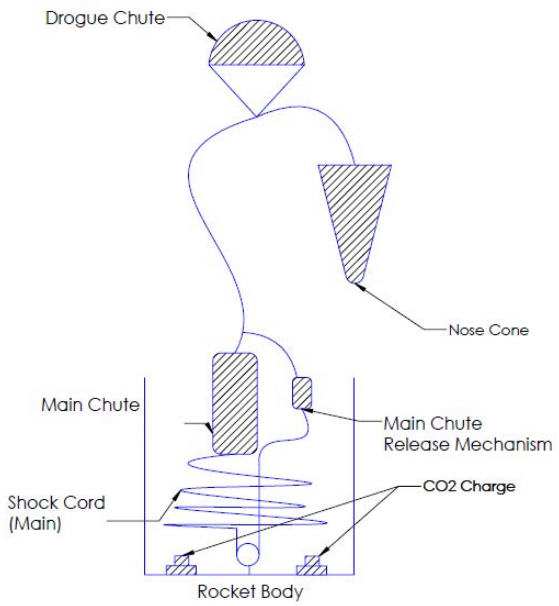

Figure 4: Rocket Descent under Drogue Chute

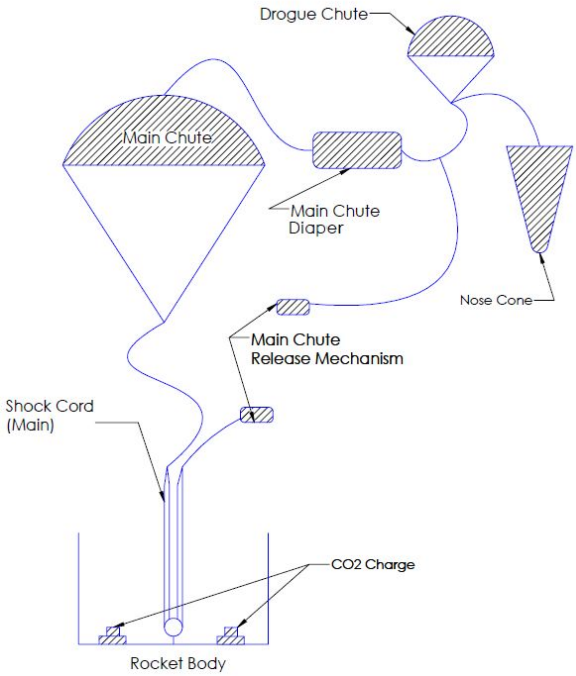

Figure 5: Rocket Descent under Main Chute

2.1 Force Calculation

Two parachute opening force methods were used in predicting the forces experienced by both the drogue parachute and the main parachute [35]. Both methods use the drag force equation to predict the parachute opening force. The first method assumes the weight of the rocket body is large enough that the opening of the parachute does not actually reduce the velocity of the rocket by a significant amount in that instant. This is called the infinite mass case and over predicts all opening force scenarios [37].

$$F = \frac{1}{1} v_o^2 \rho C_d A_p$$

The second method involves including a force reduction factor. For a small parachute with a heavy payload, the second method approaches that of the first method. However, as the canopy loading, defined as the weight of the payload over the effective drag area of the parachute, decreases, the parachute opening force predicted by the second method also decreases relative to the first method. The first method was used in designing both the main and the drogue parachutes as the overestimation of parachute opening forces predicted by this method provides a safety factor. The force calculation used for the current drogue parachute assumes a 6 sec delay after apogee. The vertical velocity reached in combination with the horizontal velocity of the rocket calculated from Open Rocket is used in determining the total drogue opening force with a predicted value of 1012lbs. The air density versus altitude for a high air density environment was taken to account for a safety factor [40]. After the drogue parachute was designed, the main parachute opening load was calculated to be 1866lbs, based on the steady state descend velocity of the drogue at 1500ft above ground level.

2.2 Drogue Parachute

A cross design was chosen for the drogue parachute based on three factors: stability, drag coefficient and ease of manufacture thereby increasing reliability. The drogue parachute reduces the rocket to a reasonable freefall velocity for the main parachute to open [35]. The minimum main parachute force is achieved by reducing the drogue

parachute steady state descent velocity while accounting for wind drift to ensure the rocket does not drift outside the designated landing zone. Maximum wind speed versus altitude was taken from an airport near Spaceport America and simulations were run to estimate the rocket drift distance. The estimated rocket weight and an estimated coefficient of drag of 0.63 were used in determining the nominal diameter of the drogue parameter and a 8.5ft nominal diameter drogue chute was selected. The estimated terminal velocity at 1500ft is predicted to be 66ft/s. The canopy fabric was chosen to reduce both oscillatory and rotational instability. It was determined that 1.1oz fabric at 80-120cfm porosity would be both strong and stable enough during descent. The canopy porosity and geometric porosity was selected to reduce rotational and oscillatory instability. See Appendix VII for engineering drawing.

The design was then further refined through the data collected by the US military tests [32-35]. With the results from the force calculation, the canopy strength was determined. The number of suspension lines as well as the line length was chosen as a trade off optimization between weight and effective drag [32]. 15ft of ¼" kevlar shock cord will be used for the drogue parachute as this provides sufficient strength during the parachute opening phase. An unfurling test of the drogue parachute was performed at running speed and the drogue opened successfully.

2.3 Main Parachute

The main chute was chosen based on its ability to bring the rocket to the ground at a safe speed. Four different designs were considered, and a conical design was chosen based on weight, stability, ease of construction, coefficient of drag, and opening force. The ease of construction originally played large influence. From an estimated drag coefficient of 0.95, the main parachute was chosen to have a nominal diameter of 25ft. This gives the rocket vertical landing velocity of 18ft/s. A low number of 16 suspension lines was chosen to reduce the chances of entanglement and to prolong the parachute opening time. The longer opening time spreads the parachute opening forces over a longer time interval. Based on the force calculations, the suspension line and canopy rating were determined. A low 0-3cfm porosity rating was selected to maintain the previously estimated drag coefficient of 0.95. The number of gores were chosen to match the number of suspension lines. Based on findings in literature, bias panels were used in the construction of the gores to better handle canopy loads [35]. The number of panels on each gore was chosen based manufacturing limitations. See Appendix VII for engineering drawing.

After consulting with the team's academic advisor, it was decided to outsource manufacturing of both the drogue and the main parachutes to increase reliability. The optimal conical angle of 27.5 degrees was chosen to maximize drag. The vent hole ratio was chosen based on the minimum size required to reduce oscillation to an acceptable amount. This value is found by comparing data from low Reynolds number parachutes with commercially available parachutes that experiences high Reynolds numbers like that by the main parachute at around 2.3e6. The main parachute will be connected to the rocket by 15ft of ½" kevlar shock cord as this provides sufficient strength during the parachute opening phase. Finally, an optimization analysis was run to minimize the main parachute weight. This was done by increasing and decreasing the suspension line length as this which varies the drag coefficient of the parachute [36].

2.4 Drogue Parachute Release Mechanism

At an altitude above 20,000ft, conventional rocketry black powder charges become unreliable [38]. A CO2 system was chosen as a suitable alternative. See Appendix VII for engineering drawing. Most of the calculations made with regards to CO2 sizing are empirical. A convention used in rocketry is to multiply the amount of black powder needed in a ground test by a factor of five [38]. Due to uncertainties associated with vent holes and other leakage points, an estimate based on previous year's rocket was used, yielding an estimated 75 grams of CO2 required. Two Raptor CO2 will be used to eject the gas as quickly as possible because the flow out of the CO2 canisters are choked. Two e-matches will be used to trigger each Raptor systems at apogee, with the first trigger coming from the student designed flight computer and a delayed signal coming from Eggtimer Quantum. The Raptor CO2 system was tested with the Eggtimer Quantum and performed as expected.

2.5 Main Parachute Release Mechanism

The main parachute release mechanism restrains the main parachute from being released until the rocket descends to an altitude of at most 1500 ft above ground level. It is based on the working concept of the commercially available tender descender, but student designed in this case to meet the specific needs of the current drogue opening force at 1012 lbs. See Appendix VII for engineering drawing. The release mechanism consists of two parts, the main body and the pin piece [39]. The main body has three holes along the main axis, with the two holes on either side of the piece being through holes. The pin piece contains three pins that fit into the main body.

The pins on either side connects to the drogue parachute and the main parachute respectively. The side that connects to the main parachute has a shorter cord than the actual main parachute shock cord and therefore prevents the main parachute from being pulled out from the parachute compartment until the release mechanism is activated. The release mechanism works through the separation of the main body and the pin piece, allowing the shorter cord to separate. The separation happens through the trigger of black powder inside the center hole. Then the main parachute can be pulled out by the drogue. The release mechanism has been tested to the drogue parachute opening shock force and performed as expected.

C. Payload Subsystems

3.1 Scientific Experiment

The scientific payload of our rocket is to observe the effectiveness of a custom material to shield against cosmic radiation. A concern for astronauts, pilots and people in other jobs where exposure to radiation is eminent is the increased dose rate they recieve. When considering how to best shield humans and other creatures from the dangerous effects of space, one must first consider what type of radiation you wish to shield against. For instance, when considering how to shield against massive particles such as alpha particles the concern is providing a thin layer of material to block the particles, as the alpha particles are damaging but easily blocked. On the other hand, high energy electromagnetic radiation is best shielded against using materials of high atomic mass. For astronauts, the protective properties would need to extend to shielding against other harsh conditions in space as well, for example the extreme temperatures and pressures. Outside of the earth's atmosphere, the radiation that you are expected to encounter is much more dangerous than the radiation that you are expected to encounter on the surface of the earth. This is because much of the radiation that you are expected to encounter when above the atmosphere is absorbed or blocked by the atmosphere. For this reason, it is very important to properly shield any biological system from dangerous sources of radiation. Some sources of radiation that are of concern include cosmic rays, radiation from the Van Allen Radiation Belts, and high intensity solar radiation rays. The payload consists of three functional units divided into three cubesat bays.

3.2 Electronics

The sensing package, i.e. the thermistors, photoresistors and such, is connected to an arduino teensy. This holds the SD card that logs all the payload sensor data. The payload radiation sensors are powered by simple but efficient Arduino Nano's running at 16MHz. To reduce the erroneous readings due to noisy output of the geiger tubes (one ionizing particle event usually produces a brief blip of noise), a denoising library is used on the Arduino. The denoising function reconciles events within a certain temporal threshold of each other into a single event, allowing us to accurately measure radiation.

3.3 Structure and Components

The upper two bays are 12 cm in height and each contain a radiation measuring unit. One of the geiger counter container is placed in the shielding material. The unshielding radiation sensor is used to record a baseline radiation profile as a function of altitude during the flight, the other is to ascertain the effectiveness of radiation shielding. The lower bay is 5 cm in height and houses the main payload computer and data logger, as well as some auxiliary sensors. The total dimensions of the payload are 10cm x 10cm x 34.1cm. Outside of the payload are ten sensors mounted into the nose cone to measure rocket rotation speed and profile the nose cone temperature gradient. A pitot tube is used to measure rocket airspeed. The three containers are separated by metal plates which have threaded rods running through them to provide structural support to the entire encasement. The payload is housed in the nose cone so as to, not only mitigate effect of the payload on the rocket but also of the rocket on the radiation sensing abilities of the payload.

Figure 6. Render of the payload contained within the Atlantis II rocket

D. Avionics Subsystems

4.1 Flight Board and Sensors (Barometer, Altimeter, IMU, GPS)

The Flight Board acts as the central system for controlling the rocket and is has been custom designed and in-house fabricated for this purpose. At the heart of the board is a STM32F4 micro-controller unit (MCU). The reasons the chip was selected are due to its low power usage compared to full OS alternatives like a Raspberry Pi, its high reliability (it has regular commercial use), and past experience as some members have successfully used it in a similar projects.

The board is connected to launch systems via an external umbilical cord which supplies two ground lines, 12V DC power, two communication channels, and a select line (active high to determine if the rocket is connected to launch systems). From this connection, the power is immediately routed to a connection to the battery board which charges the onboard LiPo battery. The battery then provides 7.4V power back to the board to power the board, GPS, radio, and pressure sensors. This centralized architecture of each component only connecting to the flight board, combined with the Molex plugs which only fit one way, simplifies the wiring on the rocket.

Directly mounted to the flight board are the barometer and the inertial motion unit (IMU) (which consists of a magnetometer, accelerometer, and gyroscope). The data from these two sensors are fed to the Kalman filter to detect apogee (see section below).

Connected to the rocket, but not on the flight board, are the GPS, two pressure sensors, and a 900 MHz long range (1 watt) radio. The pressure sensors are connected to the oxidizer tank and the combustion chamber to aid in monitoring pressures and determine what venting action is necessary. The GPS is used to determine the rocket's location, primarily to track its location upon descent and landing, and is transmitted via the onboard (transmission only) radio to a (receiving only) radio on ground station. All data generated by the collection of sensors is logged and saved to an onboard SD card for later analysis.

A diagram of all of the rocket's electrical components is available in Appendix VII.

4.2 Software Systems

The software controlling the recovery system is created with safety as the foremost priority, and uses the wide array of sensors supported by the avionics. This includes, in particular, the barometer and accelerometer as the primary tools to determine apogee and perform safety checks. There are several different levels of readiness in place to ensure that the parachutes will not deploy prematurely. All software is version controlled via Git and stored on GitHub with limited write access. All changes are subjected to a review and quality assurance (QA) process and

must pass continuous integration, an automated quality checks. The software is all linted using Astyle to promote code clarity and standards.

The software is run on the main Flight Board and is built on the FreeRTOS framework, which provides a large wealth of well-tested libraries and allows safe execution of multiple threads to ensure important processes do not interfere with unimportant processes. For example, if the logging process is malfunctioning, the process to monitor for apogee will be unaffected. In the software, all variables are either allocated on the stack or in static memory. Some data is allocated in the heap before the main loop starts and is all deallocated after the main loop. This ensures there is no memory leaks which could cause a crash after a long time. Infinite loops (other than the main loop) are prohibited, every loop must have a clear termination condition.

The software in the rocket has 6 stages: PRELAUNCH, BURN, COAST, DROGUE_DESCENT, MAIN_DESCENT, and ABORT. At any point in time, if the system receives an ABORT command via UART or the rocket is found to be in an unsafe state, the software enters the ABORT stage. All other control threads are killed, the injection is closed, parachute deployment is disabled, and the vent valve is attempted to be opened to release oxidizer and prevent any further action from the rocket. The system must be power cycled in order to leave the ABORT stage. Unsafe states include the rocket not being vertical in the BURN stages and the oxidizer tank pressure reaching super critical levels.

In the PRELAUNCH phase, the injection valve is closed, parachute deployment is disabled, the venting process is enabled, and the rocket listens for a launch command via UART from the launch system. The injection valve is closed to prevent premature combustion on the launch rail. The parachute deployment is disabled to prevent premature parachute ejection from the launch rail. The venting process monitors the pressure in the oxidizer tank and opens the vent valve if the pressure/temperature in the tank are above safe levels, this important because at this point in time the off-board launch system will be filling the tank with oxidizer during prelaunch. The rocket will also be listening for a launch command to enter the next phase, the BURN phase.

In the BURN stage, the injection valve is opened and combustion begins, this is the only stage where the injection valve is open. Parachute deployment is still disabled to prevent deployment during combustion. At this point in time the software also watches if the rocket is no longer vertical, if the rocket is no longer vertical, the ABORT stage is entered. This is to prevent a missile-like scenario, where the rocket is combusting while it is aimed horizontally. After a pre-calculated amount of time, 13 seconds, the rocket enters the COAST stage.

In the COAST stage, the injection valve is closed and the rocket prepares for apogee. The injection valve will remain closed for the remainder of the flight. Parachute deployment is now enabled and the system uses a sophisticated and well-tested Kalman filter with acceleration and pressure data to detect apogee. When apogee is detected, the drogue parachute is deployed and the system enters the DROGUE_DESCENT stage.

In the DROGUE_DESCENT stage, the system uses the Kalman filter, like in the COAST stage, to detect when an altitude of 1500ft is reached. When that altitude is reached, the main parachute is deployed and the system enters the MAIN_DESCENT phase.

In the MAIN_DESCENT phase, the system is mostly idle as this is the terminal stage. The system's main task will be to reliably send GPS coordinates back to mission control to facilitate recovery.

During all stages, the system is reading acceleration, gyroscope, magnetism, barometer, GPS, oxidizer tank pressure, and combustion tank pressure data. It is also monitoring for emergency shut off (entering the ABORT stage), logging data to an SD card, and transmitting data via UART to the radio.

4.3 Battery Boards & Battery

The battery used to control the rocket's avionics system is a 7.4V two-cell lithium polymer and board has be designed for a battery of this specification. The primary component of the battery board is an off the shelf battery charging chip (an MCP73213 OVP Dual-Cell Li-Ion Battery Charger) which protects the battery during charging and discharging. Some of its features include overvoltage protection, automatic charge termination, and thermal regulation. The board also has switch terminals for the power and battery input, and a molex connector so it can be connected to the main flight board. A schematic of the board can be found in APPENDIX VII

4.4 Kalman Filter

The on-board Kalman filter is tuned to the specific conditions of the launch. We expect to go supersonic, and so we have correspondingly decreased the dependence of the algorithm on the barometer to avoid transient behaviour introduced when travelling at transonic speeds. The accelerometer then becomes the primary source to minimize our error when comparing to our real-world state. An added benefit of the Kalman filter is that it also allows us to filter

out white noise to an extent, all while maintaining near real-time responses.

As mentioned above, the Kalman filter is used to detect apogee during the COAST stage. By looking for zero velocity within a tolerance, we have tuned the algorithm to send the signal to release the parachute slightly before apogee, even with the modest delay compared to real-world altitude by 0.1 seconds. This allows the parachute to unfurl at exactly the right moment to reduce stress on the airframe and parachute itself.

The Kalman filter also allows us to trivially deploy the main parachute on time, during the DROGUE_DESCENT stage, by looking for any altitude lower than our deployment altitude. This does not face nearly as many challenges as detecting apogee, since there is a large window where the parachute can be deployed safely without inducing too much drift.

E. Propulsion Subsystems

Figure 7. Oxidizer Tank and Propulsion System

5.1 Oxidizer Tank

A large tank is required to contain the nitrous oxide propellant. It is stored in a two-phase gas-liquid mixture. No turbo pump is required in the feed system as nitrous oxide is self-pressurizing due to its high vapor pressure. The maximum expected operating pressure is 1000 psi and this is controlled by a pressure safety valve mounted on top of the vessel which is set to 1000 psi. The design temperature of the Nitrous oxide is 25 , chosen to match known test conditions and to be distanced from the critical temperature of 36.4 . In order to regulate the temperature in a hot environment, nitrous oxide will be vented from the flight tank before it reaches the critical temperature, experiencing cooling by expansion. The N2O mother bottle will be stored at a temperature below its critical temperature in an insulated shack with a cooling system.

5.1.1 Analysis and Design

The flight tank is a SRAD composite overwrapped pressure vessel (COPV). The vessel is an external tank and a structural member of the airframe. The vessel consists of an aluminum liner, isotensoid end caps with polar ports on either end. The vessel is comprised of 2 helical and 4 hoop layers. simulations were completed in ANSYS with ACP. The fiber buildup and angle was formulated based off of literature values and imported into an ANSYS simulation. A MATLAB script was used to generate the data for a look-up table (fiber orientation, volume, and fiber-epoxy ratio). The vessel was designed for a burst pressure of 3000 psi or 3x the maximum expected operating pressure (MEOP) of 1000 psi. Additional analysis details are presented in Appendix VI. The composite and filament properties were acquired from our local branch of Luxfer gas cylinders who agreed to help us construct it.

The ⅛” 6061-T6 COPV liner was welded with 4943 filler rod and heat treated back to a T6 temper before being filament wound. Since the epoxy resin used in our COPV cures at 250 and the fact that carbon has a much lower coefficient of thermal expansion than aluminum, the liner shrinks away from the overwrap at room temperature (delamination), but contacts at a pressure under MEOP. The common industry solution to delamination is to autofrettage (yield) the liner back into the overwrap such that the liner is in residual compressive stress at zero pressure. Our ANSYS simulations show autofrettage does not occur at our proof load. A maximum principal stress failure does not occur at 3x MEOP with our liner and overwrap design.

Simulation results are available in Appendix VI

The drawings for the oxidizer tank are available in Appendix VII : COPV, COPV01, COPV02

5.2 Injector and Feed System

The feed and injection system contains all the necessary components to transport the oxidizer from the oxidizer tank into the combustion chamber. Along this system, the oxidizer is restricted to an appropriate flow rate and is atomized during injection into the combustion chamber to help facilitate combustion.

One of the difficulties encountered during the project was the selection of an appropriate valve system to control the oxidizer flow rate to the combustion chamber. One of the attractive features of hybrid rockets is the relative simplicity of implementing throttle control during operation of the motor, however in this project this avenue was

not explored. The difficulty in our system arose from the necessity of supplying high mass flow of 1.6 kg/s while maintaining a lightweight and flightworthy design that could fit into a 7” body tube. There are two main valve considerations that could fulfil these requirements.

Our first option we considered was the design of the previous vehicle, Atlantis I, injection system. The design split the flow into three lines which would connect to three solenoid valves. Each solenoid would have the capability of roughly 0.5 kg/s during a burn, based off of previous tests of the Atlantis I engine. Splitting and recombining the flow into three lines adds additional losses and more leak points and complexity.

A single compact lightweight valve-actuator assembly was sourced from Assured Automation. This valve consists of: a ball valve, an actuator, a solenoid valve and a working gas. In our case the working gas is a CO2 canister regulated to 100 psi.

The drawings for the final injector assembly are presented in APPENDIX VI as INJE01

Figure 8. Assembled injector assembly with valves attached - full and cross-sectioned view

The challenges associated with predicting the nitrous oxide mass flow rate arise primarily from the fact that the liquid nitrous oxide is in a saturated state when it leaves the oxidizer tank. This means that the liquid exists in an equilibrium with its vapor phase and will begin to boil if the pressure in the liquid drops. As a result the entire process must be treated as a two phase flow problem, and the estimation of mass flow rates through valve and orifices must be treated as a two state flow.

The Injection system was assumed to have negligible losses until the injector plate which consists of 30 to 50 1.5 mm diameter holes. The 1.5 mm holes were chosen as they have been known to sufficiently atomize the flow [18]. The flow was modeled through the following set of equations. State 1 is before the injector plate and state 2 is after. The flow was assumed to be isenthalpic through the plate. The physical meaning of G is mass flow per unit area.

$$G = \frac{\kappa G_{SPI} + G_{HEM}}{1 + \kappa}$$

$$G_{SPI} = C_d \sqrt{2\rho_1 (P_1 - P_2)}$$

$$G_{HEM} = C_d \rho_2 \sqrt{2(h_1 - h_2)}$$

$$\kappa = \sqrt{\frac{P_1 - P_2}{P_{1,sat} - P_2}}$$

Since the discharge coefficient is an empirical value ranging from 0.3 to 0.9 [18] the injector plate will be tuned to the design mass flow of 1.6 kg/s after successive tests. The plate has the capacity for 55 holes that our countersunk. The number of holes through drilled is not known during the writing of this document. An efficient method of placing the holes equidistant is hexagonal packing. The injector plate was mounted to an injection assemble that was radially bolted to the chamber and sealed with circumferential o-rings.

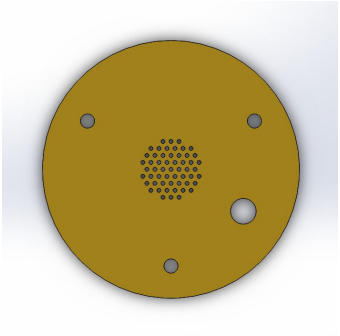

Figure 9. Injection plate showing the number and placement of 1.5mm hole

5.3 Combustion Chamber

The combustion chamber contains two major subassemblies, the combustion casing and the fuel cartridge. The arrangement of the assembly can be seen in the adjacent. As an assembly, this section of the rocket motor is the location in which the reaction between the fuel and the oxidizer takes place. The purpose of this section is to contain and direct the flows created by this process. The combustion reaction produces high temperatures and pressures that are typically controlled by flow properties upstream and downstream of the combustion chamber.

The chamber consists of a 6" OD x 0.125" wall x 23.5" 6061-T6 structural aluminum tube with 12 radial clearance holes for cap screws to retain the injector plate and nozzle housings. Inside the chamber is the fuel cartridge consisting of a 5" nominal PVC pipe wrapped in a sheet of LDPE that is epoxied to the PVC pipe. Inside the pipe there are two layers of 1/16" EPDM insulation. The fuel length is 14" with a 2" pre and a 3.5" post combustion chamber. The chamber's MEOP (maximum expected operating pressure) is 350 psi.

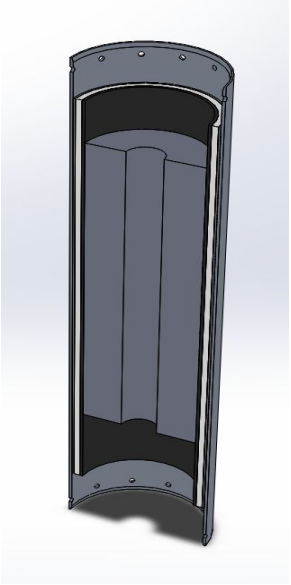

Figure 10. Cross Section of Combustion Chamber Showing Insulation and Fuel Grain

The radial and axial plane stress state of the cylinder is resolved into the following expression from thin walled pressure vessel theory . [31]:

$$\sigma = \frac{Pr}{t}$$

Using the yield stress as the maximum allowable stress, and the vessel thickness and radius, a safety factor of 4.0 is achieved with regard to the pressure.

The strength of the radial bolts and vessel bearing capacity was considered. An internal pressure of 2 x MEOP was used to design the bolt holes, number, and spacing. The resolved force of the 2x MEOP on the projected area requires each end connection to withstand 18494 lbs of force. This force was resolved into twelve, #12-24, equally spaced bolts, a more manageable requirement of 1541 lbf bearing capacity was required for each bolt. The bolts have a shear capacity of 2126 lbf [30]. The aluminum wall bearing stress was calculated using the formula:

$$\sigma = \frac{F}{dt}$$

The ultimate bearing strength of aluminum for 2.0 x diameters away was used as the maximum allowable stress. For a #12 bolt clearance the safety factor is 2.47. A hydro-test was performed at a proof load of 525 psi or 1.5x the MEOP on the combustion chamber for a time of 10 minutes. No ruptures or leaks were observed.